Trace Level Determination of Lead in Solid Samples by UV Laser Ablation and Laser-Enhanced Ionization Detection

ARTICLE *in* ANALYTICAL CHEMISTRY · APRIL 2003

Impact Factor: 5.64 · DOI: 10.1021/ac026223k · Source: PubMed

3 AUTHORS, INCLUDING:

Jean-Francois Gravel
National Optics Institute
13 PUBLICATIONS **121** CITATIONS

SEE PROFILE

Denis Boudreau
Laval University
49 PUBLICATIONS **1,435** CITATIONS

SEE PROFILE

Anal. Chem. **2003,** *75,* 1442−1449

Trace Level Determination of Lead in Solid Samples by UV Laser Ablation and Laser-Enhanced Ionization Detection

Jean-François Gravel, Philippe Nobert, Jean-François Y. Gravel, and Denis Boudreau*

Department of Chemistry, Université Laval, Québec City (PQ) Canada G1K 7P4

Laser-enhanced ionization was investigated as a detection technique for trace elemental analysis of solid samples by laser ablation. Laser ablation of aluminum samples was performed in an ablation cell, and the ablated material was carried by a flow of gas to a miniature LEI flame where Pb was detected. This decoupling of ablation cell and detector allowed the independent optimization of vaporization and detection processes. We have investigated the different excitation schemes for Pb and uncovered five new LEI-active transitions in the visible range. We have demonstrated that the use of an argon−oxygen/acetylene flame sheathed with argon resulted in the elimination of background interference from the two-photon ionization of nitric oxide. We have shown that the use of helium as a carrier gas results in a higher ablation yield and lower pulse-to-pulse variations in LEI signal and in better analytical figures of merit. We have characterized the performance of the technique in terms of detection limits and dynamic range, and we have obtained a detection limit of 60 ng/g for the determination of Pb in high purity aluminum.

The interest in the use of laser ablation for elemental analysis has grown tremendously over the past few years, fuelled by the numerous advantages it provides for the direct analysis of solid samples.[1,2] Since dissolution of the sample is not needed, the sample preparation procedures are minimal, which results in reduced risks of contamination, lower analysis costs, and higher sample throughput. In addition, the small footprint of the laser beam focused at the sample surface allows spatially resolved analysis of heterogeneous samples with micrometer resolution in both the lateral and depth dimensions. Picogram to nanogram amounts of ablated sample material have been measured using a number of techniques, most notably inductively coupled plasma mass spectrometry (ICP-MS) or atomic emission spectrometry (ICP-AES)[2], laser-induced breakdown spectrometry (LIBS),[3] laser-excited atomic fluorescence spectrometry (LEAFS),[4] and laser atomic absorption spectrometry (LAAS).[5]

A detection technique that is well-suited for the analysis of the minute amount of material sampled by laser ablation is laser-enhanced ionization (LEI).[6] It is based on the selective laser excitation of analyte atoms to a high-lying state by tunable laser(s), followed by thermal ionization, usually in an air/acetylene flame in which the sample has been introduced, and detection of the resulting charges. When excitation proceeds through favorable atomic transition(s) that lead to excited states lying sufficiently close to the ionization threshold, ionization and charge collection efficiencies are believed to be almost unity,[7] and the smallest measurable analytical signal is then determined by the fluctuations in the current carried by the native charges in the flame. Estimates for the ultimate limit of detection (LOD) attainable by LEI for aqueous solutions in a typical experimental setup range from the low femtogram per milliliter to picogram per milliliter levels, depending on the degree of atomization of analyte species in the flame, the occurrence of thermal ionization of matrix species, or interference from instrumental noise sources.[8,9]

The extremely high sensitivity of LEI makes it well-suited for microanalysis at the trace level, in particular when the limited amount of sample material and low analyte concentrations exclude sample dilution and analyte preconcentration procedures. Exceptional results have been obtained in this area by coupling the LEI flame detector to discrete sample vaporization devices, such as electrothermal atomizers based on the graphite rod or furnace, resulting in LODs reaching 4.2 pg/mL of Pb in diluted blood (42 fg in a 10 μL injection volume)[10] or 1 pg/g of indium in a solid sample with a mass of 10 mg.[11] However, the use of LEI as a detection technique for laser ablation has not yet been thoroughly investigated. As was reported by Pang and Yeung,[12] LEI detection cannot be performed directly in the laser plasma plume, because the high local temperature results in a high background current from the thermal ionization of analytes and matrix components alike and also because spectral resolution is severely degraded

* To whom correspondence should be addressed: Phone: (418) 656-3287. Fax: (418) 656-7916. E-mail: denis.boudreau@chm.ulaval.ca.

(1) Niemax, K. *Fresenius' J. Anal. Chem.* **2001**, *370*, 332−340.
(2) Russo, R. E.; Mao, X.; Liu, H.; Gonzalez, J.; Mao, S. S. *Talanta* **2002**, *57*, 425−451.
(3) Radziemski, L. J. *Spectrochim. Acta* **2002**, *57B*, 1109−1113.
(4) Gornushkin, I.; Baker, S. A.; Smith, B. W.; Winefordner, J. D. *Spectrochim. Acta* **1997**, *52B*, 1653−1662.
(5) King, L. A.; Gornushkin, I. B.; Pappas, D.; Smith, B. W.; Winefordner, J. D. *Spectrochim. Acta* **1999**, *54*, 1771−1781.
(6) Boudreau, D.; Gravel, J. F. *Trends Anal. Chem.* **2001**, *20*, 20−27.
(7) Omenetto, N.; Smith, B. W.; Hart, L. P. *Fresenius' J. Anal. Chem.* **1986**, *324*, 683−697.
(8) Matveev, O. I.; Omenetto, N. *AIP Conf. Proc.* **1995**, *329*, 515−517.
(9) Turk, G. C. *Laser-Enhanced Ionization Spectrometry*; Travis, J. C., Turk, G. C., Eds.; John Wiley and Sons: New York, 1996; p 186.
(10) Riter, K. L.; Matveev, O. I.; Smith, B. W.; Winefordner, J. D. *Anal. Chim. Acta* **1996**, *333*, 187−192.
(11) Chekalin, N. V.; Pavlutskaya, V. I.; Vlason, I. I. *Spectrochim. Acta* **1991**, *46*, 1701−1709.
(12) Pang, H. M.; Yeung, E. S. *Anal. Chem.* **1989**, *61*, 2546−2551.

10.1021/ac026223k CCC: $25.00
Published on Web 02/08/2003

by pressure-broadening effects. More recently, Gorbatenko et al.[13,14] reported on the development of a hybrid technique in which a solid sample was placed directly below the combustion zone of a specially designed air/acetylene flame. Ablation of aluminum alloy samples was performed with the second harmonic of an Nd:YAG laser (532 nm), and lithium was detected by two-step excitation ($\lambda_1 = 670.784$ nm and $\lambda_2 = 610.362$ nm). Although this close coupling reportedly minimizes sample losses during transport to the flame, electrical interference from charged species originating in the laser plasma requires a certain temporal separation to be maintained between the ablation and excitation laser pulses.[14] No analytical figures of merit were given.

The purpose of the present work is to couple laser ablation and LEI detection (LA-LEI) for the direct trace analysis of solid samples using an ablation cell separated from the LEI flame by a transfer line akin to systems used in laser ablation ICP-MS. This hybrid configuration avoids the contribution to the overall analytical signal of thermions generated by the ablation event while allowing the independent optimization of both vaporization and detection processes. Laser ablation of solid samples was performed using an excimer laser at 308 nm, and the vaporized material was carried by a flow of argon or helium from the cell into a miniature flame, where Pb was detected at the trace level using a two-step excitation scheme ($\lambda_1 = 283.305$ nm and $\lambda_2 = 508.948$ nm). This miniflame, inspired from a design developed by Smith et al. for GF-LEI work,[15] is well-adapted to laser ablation, since it involves a much smaller dilution factor than other atom reservoirs and provides the high sensitivity required by the few tens of nanograms of material ablated by each laser shot.

EXPERIMENTAL SECTION

Laser System. An excimer laser operated in XeCl at 308 nm at a pulse repetition rate of 30 Hz (model PM-846, Lumonics), was used to simultaneously pump two dye lasers (models EPD-330 and HD-300, both from Lumonics) and to ablate solid samples in the ablation cell. The dyes used were Sulphorodamine B (Lambda-Physik) in the region of 600 nm and Coumarin 500 and Coumarin 540A (Exciton) in the regions of 510 and 285 nm, respectively, the latter following frequency doubling of the 570-nm fundamental in a KDP crystal. Pulse energy from the excimer laser and the dye lasers was measured with thermopile and pyroelectric probes connected to an energy/power meter, respectively (models PM150-50XB, J9-LP, and EPM1000, respectively, all from Molectron).

Laser Ablation Optics. Part of the excimer laser beam was imaged onto the sample surface using a circular beam mask and a short (30-mm) focal length triplet lens corrected for spherical aberration (model 54-17-30, Special Optics, Wharton, NJ). With a demagnification ratio of ~25 and a mask aperture diameter of 6 mm, this optical setup provided a beam diameter on the sample surface of ~240 μm and ablation craters of fairly regular shape and energy profile, with a beam irradiance independent of mask size and controllable via the excimer laser power supply and beam splitters upstream of the beam mask. With a typical excimer laser pulse energy of ~200 mJ and ~50% of this being directed into the dye lasers, the remaining pulse energy through the 6-mm iris (8 mJ) resulted in a beam irradiance of 0.6 GW/cm^2 at the sample surface.

Ablation Cell. The internal volume of the ablation cell was profiled in order to maintain laminar flow and minimize turbulences and was made as small as possible to minimize dead volume. The samples were introduced into the cell from the bottom using a spring-loaded platform to keep the surface of each sample at a constant distance from the lens, as required by the short depth of field of the triplet lens. A photodiode mounted below the spring-loaded platform allowed us to determine the number of pulses needed to pierce thin aluminum samples and, thus, compare ablation speed as a function of ambient gas composition. The ablated particles were carried to the LEI flame via a 4-m-long, 1/8-in.-i.d. Tygon tubing by a flow of argon or helium gas. The optimal carrier gas flow rate is a compromise between increased losses of larger particles to gravitational settling at lower flow rates and decreased particle atomization due to an insufficient residence time in the flame at higher flow rates as well as to a decreased probing efficiency of the shorter analyte transient due to the finite duty factor of the dye laser system. For the current work, the optimal carrier flow rate varied between 0.4 and 0.7 L/min, depending on sample type.

For the optimization of the excitation scheme of Pb and for the flame temperature determination experiments, an ultrasonic nebulizer (model U-5000AT+, CETAC Technologies) was used in place of the ablation cell to provide a constant input of analyte particles to the LEI flame. Measurement of the ablation yield as a function of ambient gas composition was done by weighing on a microbalance milligram-size aluminum samples before and after ablation runs. For each measurement, ablation was performed with the imaging mask removed and using a long-focal-length plano–convex lens for many pulses and in many craters—in order to reach a sufficient ablated mass (a few micrograms)—and the total mass loss was divided by the number of ablation pulses. Care was taken to ensure that the width-to-depth ratio of the ablation craters was large enough to avoid a plasma confinement effect that could alter the ablation rate.[16]

Particle Characterization. To examine the shape and size distribution of ablated particles, the latter were collected on Nucleopore polycarbonate membranes (0.1-μm pore size, Structure Probe Inc., West Chester, PA) using a short (~20 cm), straight section of Tygon tubing, an in-line stainless steel filter holder (model P-02929-10, Labcor), and a small vacuum pump (model 400-1901, Barnant Company, Barrington, IL) downstream of the membrane to compensate for the pressure drop caused by the in-line filter.[17] The carrier gas (argon or helium) was first sent through an in-line 0.2-μm absolute filter (DFA Emflon II cartridge assembly, Pall Corporation), and SEM of blank Nucleopore membranes (sampling of the carrier gas without any ablation) showed no remaining particles in the carrier gas stream.

Flame Apparatus. The premixed air/acetylene and argon–oxygen/acetylene flames were supported on a custom-made

(13) Gorbatenko, A. A.; Zorov, N. B.; Kuzyakov, Y. Y.; Murtazin, A. R. *J. Anal. Chem.* **1997**, *52*, 490–492.
(14) Gorbatenko, A. A.; Zorov, N. B.; Murtazin, A. R. *J. Anal. Chem.* **2002**, *57*, 125–130.
(15) Smith, B. W.; Petrucci, G. A.; Badini, R. G.; Winefordner, J. D. *Anal. Chem.* **1993**, *65*, 118–122.
(16) Eggins, S. M.; Kinsley, L. P. J.; Shelley, J. M. G. *Appl. Surf. Sci.* **1998**, *127–129*, 278–286.
(17) Baker, S. A.; Smith, B. W.; Winefordner, J. D. *Appl. Spectrosc.* **1998**, *52*, 154–160.

concentric miniburner. It is based on a design proposed by Smith et al.[10] to which was added an external gas channel allowing the use of an argon sheath in order to reduce the back-diffusion of atmospheric gas species into the flame. The gas flow rates for the air/acetylene flame were 1.7 L/min for air and 190 cm^3/min for C_2H_2, while those for the argon−oxygen/acetylene flame (see discussion) were 3 L/min for the $Ar-O_2$ mixture (Ar/O_2 ratio, 80/20) and 330 cm^3/min for C_2H_2. The argon sheathing gas was set at 1.6 L/min. All flame and carrier gas flows were controlled with mass flow meters. An 800 V electric field was established between the burner head and a water-cooled electrode immersed in the flame and consisting of a 1/8-in.-o.d. stainless steel tube, at a distance of 2 cm from the burner head. The dye laser beams were directed into the miniflame immediately below the electrode and aligned for spatial and temporal coincidence. The charges created in the flame were collected at the burner central tube and sent first through a high-pass filter (cutoff frequency ∼ 30 kHz) and then to a custom-made AC-coupled transimpedance preamplifier (gain of $\sim 10^5$ V/A). The resulting voltage was fed to a boxcar integrator (model SR250, Stanford Research Systems). Data acquisition and system control was performed with a PC interface and software written in Labview 5 (National Instruments).

Temperature Measurements. Flame temperature determination was performed by optical emission measurements using the two-line method described in detail elsewhere,[18] using a 0.5-m monochromator (f/8.6, dispersion of 1.6 nm/mm at the exit plane, model 82-500, Jarrell-Ash) equipped with a PMT (model R928, Hamamatsu). A bias voltage of −900 V was applied on the PMT photocathode (HV source model PS325, Stanford Research Systems), and the anode current was sent to a preamplifier (model SR570, Stanford Research Instruments) prior to data acquisition and processing. During the experiments, the concentration of the probe species (e.g., iron) was kept low enough to ensure that the emission lines used for temperatures calculations were not affected by self-absorption.

Reagents and Solid Sample Preparation. Aqueous Pb solutions were prepared from a 1000 μg/mL standard stock solution (spectrometric grade, SCP Science) and 18 MΩ deionized water acidified with 2% (v/v) high purity nitric acid (Anachemia). The Fe aqueous solutions used for the temperature determination experiments were prepared by dissolving $(NH_4)_2Fe(SO_4)_2 \cdot 6H_2O$ (Fisher Scientific) in 18 MΩ deionized water acidified with 2% (v/v) high purity hydrochloric acid (Anachemia). The solutions were introduced into the LEI flame with the ultrasonic nebulizer, using argon as the carrier gas at a flow rate of 280 cm^3/min. For the laser ablation experiments, high-purity aluminum solid standards (∼20 mm long × ∼8 mm wide × ∼5 mm thick) of known composition were provided by Alcan International (CRDA, Jonquière, QC, Canada). Samples were rough-polished using 400 grit sandpaper, fine-polished using 4/0 polishing paper, and cleaned with ethanol prior to ablation. The Pb−Sn alloy samples (55% Pb in weight) used for the ambient gas composition measurements were prepared in-house.

RESULTS AND DISCUSSION

Optimization of the Excitation Scheme of Pb. LEI detection of Pb has been studied by several research groups in the past, mostly using the transition at 283.305 nm, which is the only allowed transition proceeding from the $6p^2\ ^3P_0$ ground state and within the wavelength range easily accessible to dye lasers (three other LEI-active transitions have been observed in the 280−287 nm region, but they originate from the thermally populated $6p^2\ ^3P_2$ at 10650 cm^{-1}, hence offering poorer sensitivity[9]). Since the $6p7s\ ^3P_1^\circ$ excited state populated by the 283.305-nm transition lies 3.04 eV away from the ionization limit, one-step excitation schemes for Pb do not provide optimal ionization efficiency, and the lowest limits of detection (LOD) have therefore been obtained using two-step excitation schemes, most of them using the second excitation step at 600.186 nm ending in the $6p8p\ ^3D_2$ state (ΔE_{ion}= 0.98 eV).[19] Riter et al.[20] have recently uncovered three new two-step schemes, with the second step occurring in the 500−510 range, between the $6p7s\ ^3P_1^\circ$ intermediate state and the 6p9p excited manifold lying at ∼55 000 cm^{-1}, or ∼0.6 eV, away from the ionization limit.

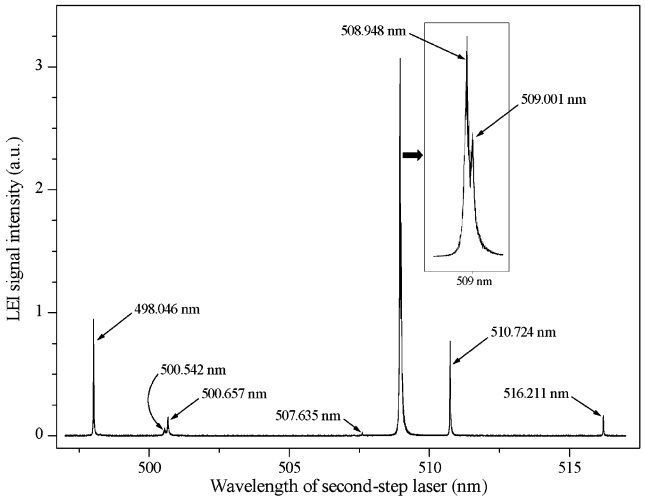

Figure 1. LEI spectrum for 2-step excitation of 25 ng/mL Pb (ultrasonic nebulization, first excitation step at 283.305 nm).

During our investigation of this spectral region, we were able to uncover five new LEI-active lines previously unreported in the literature. Figure 1 shows the LEI spectrum of Pb obtained by scanning the 497−517-nm range with the second step laser (all transitions observed in this spectral window are given in Table 1), while all Pb LEI-active transitions observed during this work are shown in the partial energy diagram in Figure 2.

In contrast to the findings of Riter et al.,[20] who reported a single line at 509.0 nm, we observed two closely spaced transitions (see inset of Figure 1), ending in states $6p9p\ ^3P_{1,2}$. These two lines were also observed by optical emission, in a paper by Wood and Andrews[21] published 10 years later than the seminal work of Moore.[22] The relative emission intensity for the two lines given in ref 21 and our own data suggest that the transition identified by Riter et al. as the most sensitive pathway to collisional ionization is the one at 508.948 nm. Similarly, the wavelength of the transition observed in ref 20 at 500.5 nm and identified as the one between states $6p7s\ ^3P_0^\circ \rightarrow 6p9p\ ^3P_1$ should rather be 500.657 nm (again,

(18) Kirkbright, G. F.; Peters, M. K.; Sargent, M.; West, T. S. *Talanta* **1968**, *15*, 663−675.

(19) Ke, C. B.; Lin, K. C. *Anal. Chem.* **1999**, *71*, 1561−1567.

(20) Riter, K. L.; Matveev, O. I.; Castle, B. C.; Smith, B. W.; Winefordner, J. D. *AIP Conf. Proc.* **1997**, *388*, 431−434.

(21) Wood, D. R.; Andrew, K. L. *J. Opt. Soc. Am.* **1968**, *58*, 818−829.

(22) Moore, C. E. *Natl. Bur. Standards (U.S.)* **1958**, *Circ. 467*.

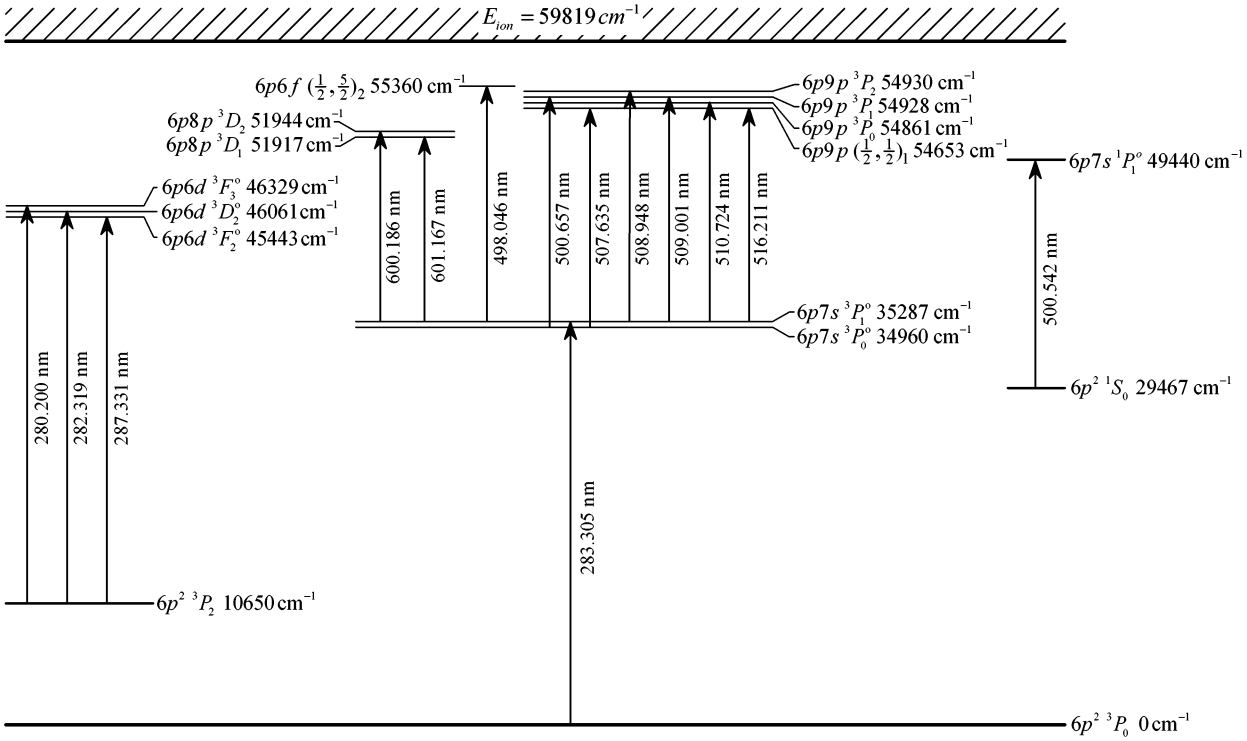

Figure 2. Partial energy level diagram for Pb.

Table 1. LEI-Active Transition Wavelengths of Pb in the Range 497−517 nm

transition wavelength[a] (nm)	configuration and term[b] of upper level	energy (cm^{-1})	E.F.[c]
498.046	6p6f$((1/2),(5/2))_2$	55360	370
500.542[d]	6p7s $^1P_1^o$	49440	12
500.657	6p9p $^3P_1$	54928	51
507.635	6p9p$((1/2),(1/2))_1$	54653	8
508.948	6p9p $^3P_2$	54930	985
509.001	6p9p $^3P_1$	54928	558
510.724	6p9p $^3P_0$	54861	275
516.211	6p9p$((1/2),(1/2))_1$	54653	83

[a] Italics indicates new LEI-active transitions. Unless noted otherwise, the first-step transition is $6p^2\,^3P_0 \rightarrow 6p7s\,^3P_1^o$, 283.305 nm. [b] Taken from Moore,[22] when available (see text). [c] Enhancement factor (signal for two-step/signal for one-step). [d] From a thermally populated level.

according to ref 21), the line observed at 500.542 nm originating instead in the thermally populated state $6p^2\,^1S_0$ (the *JS* coupling terms in Figure 2 and Table 1 were taken from Moore and are given here for reference only, because Woods and Andrews have shown that even the $6p^2$ ground configuration of Pb is nearer to *jj* than *LS* coupling). In addition, Riter et al. attributed the 498.046 nm line to the transition $6p7s\,^3P_0^o \rightarrow 6p9p\,^3D_2$, whereas Wood and Andrews found the upper level of this transition to belong instead to the 6p6f configuration. Finally, two of the previously undocumented LEI transitions observed in the present work, at 507.635 and 516.211 nm, terminate in the 6p9p$((1/2),(1/2))_1$ level, which was reported by Wood and Andrews but is absent from ref 22.

The enhancement factors (i.e., LEI signal for two-step/LEI signal for one-step) measured for all the lines observed in the present work are given in Table 1. In accordance with the results reported by Riter et al., we found that the $6p7s\,^3P_1^o \rightarrow 6p9p\,^3P_2$ transition at 508.948 nm gives the highest enhancement factor and, therefore, the largest sensitivity for the LEI detection of Pb. This excitation scheme was, thus, used for the remaining measurements.

Optimization of LEI Flame Composition. Despite the higher sensitivity and spectral selectivity that two-step excitation schemes provide, they may still be affected by background signal interferences, particularly when the first excitation step lies in the UV region, where the background signal from the multiphoton ionization (MPI) of species such as O_2, CO, and NO may degrade the signal-to-noise ratio. In the spectral region below 285 nm, nitric oxide molecules can be directly photoionized from low-lying thermally populated vibrational states by a two-photon process through the $A^2\Sigma^+$ intermediate state. The LEI spectrum shown in Figure 3, obtained in an air/acetylene flame by scanning one laser around 283.5 nm without sample introduction, shows several NO bands belonging to the $^2\Sigma\ (v' = 0) \leftarrow {}^2\Pi_{1/2,3/2}(v'' = 5)$bandhead,[23] one of which (indicated by the arrow) directly overlaps with the first-step transition of Pb at 285.305 nm. Since the intensity of this background interference scales as the square of the laser irradiance, it is inherently noisier than the LEI signal and hinders the maximization of the signal-to-noise ratio by optically saturating the involved transition(s) at high laser irradiance. Therefore, to reduce the contribution of NO photoionization to the overall LEI signal for Pb, a mixture of oxygen and argon (20:80) was used instead of air as the oxidant.[24] It was found that, while this substitution results in a decrease of ∼50% in background intensity (Figure 4, curves A and B), the NO signal

(23) Mallard, W. G.; Miller, J. H.; Smyth, K. C. *J. Chem. Phys.* **1982**, *76*, 3483−3492.
(24) Elwood, S. A.; Chekalin, N. V.; Ezer, M.; Pacquette, H. L.; Swart, D. J.; Simeonsson, J. B. *Appl. Spectrosc.* **1999**, *53*, 1237−1243.

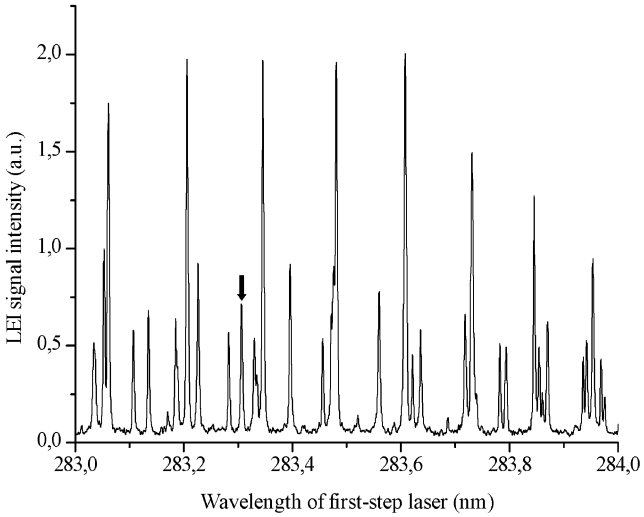

Figure 3. LEI background spectrum showing two-photon ionization of nitric oxide (NO) between 280 and 285 nm. Arrow indicates interference with LEI transition of Pb at 283.305 nm; excitation energy is 160 μJ.

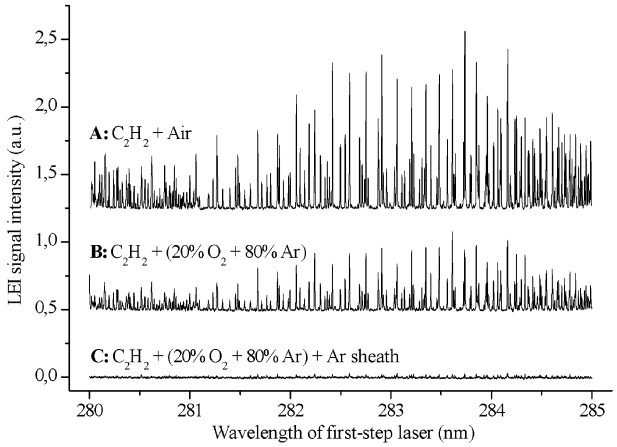

Figure 4. Effect of LEI flame gas composition on the TPI spectrum of NO (A, air/C_2H_2; B, O_2 (20%) + Ar (80%)/C_2H_2; C, O_2 (20%) + Ar (80%)/C_2H_2 + Ar sheath).

Table 2. Effect of Flame Composition on LEI Signal Intensity and Background[a]

flame composition	SD on background signal (V)	sensitivity (V/μg·mL^{-1})
air/C_2H_2	0.0019	0.0117
Ar−O_2/C_2H_2	0.0010	0.0369
Ar−O_2/C_2H_2 w/Ar sheath	0.0006	0.0359

[a] 1 μg/mL aqueous Pb, 1-step excitation at 283.305 nm, 120 μJ excitation energy.

is still significant, owing to the diffusion of ambient air from the flame periphery. We found that the use of an argon sheath gas around the flame at an optimal flow rate of 1.6 L/min virtually eliminates the remaining NO from the LEI spectrum and results in a much lower background (Figure 4, curve C). Table 2 shows a comparison of the three flames in terms of LEI signal sensitivity measured with 1-step excitation at 283.305 nm and ultrasonic nebulization of a 1 μg/g Pb aqueous solution, as well as standard deviation of the signal background from nebulization of a blank

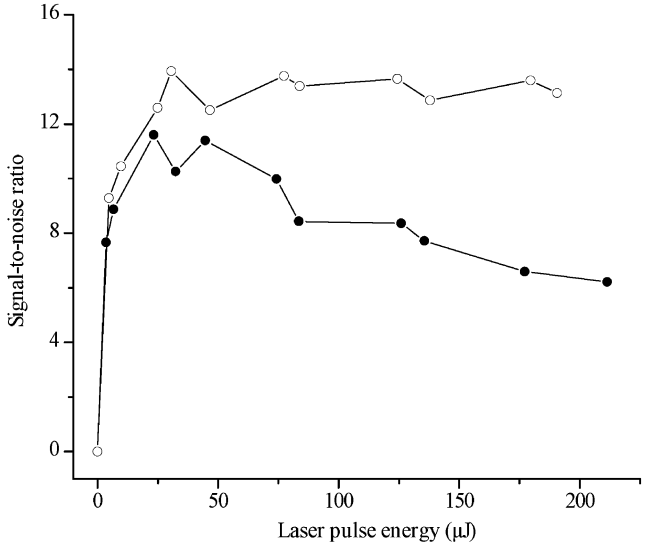

Figure 5. Effect of flame gas composition on S/N ratio as a function of excitation energy (○, Ar−O_2/C_2H_2 + Ar sheath; ●, Air/C_2H_2).

(2% HNO_3) solution. These results show that the use of the sheathed Ar−O_2/C_2H_2 flame greatly minimizes the background signal fluctuations, reducing the standard deviation on the background signal by a factor of 3 in the modified flame, which in turn results in higher signal-to-noise ratios at higher laser pulse energies (Figure 5). This benefit will be of even greater importance for the determination by LEI of elements that do not possess favorable transitions proceeding from the ground state and that must be excited via less favorable transitions requiring higher laser fluence to reach optical saturation.

In addition to this decrease in background signal fluctuations, the use of the argon−oxygen mixture resulted in an increase in LEI sensitivity by a factor of ~3 (Table 2), comparable to increases of 2−6 reported for other elements.[24] The temperatures of the air/acetylene and argon−oxygen−acetylene flames were estimated at 2430 K ± 50 and 2570 K ± 40, respectively, measured immediately below the immersed electrode using the two-line method described in the Experimental Section. Although this slight increase in temperature might reflect the more abundant thermal energy provided by the argon−oxygen mixture for atomization and ionization of the analyte species, additional experiments are needed to elucidate this effect.

The detection limit (3σ) attained for Pb, obtained using this argon-sheathed argon−oxygen/acetylene flame and the two-step excitation scheme discussed previously and using standard aqueous solutions ultrasonically nebulized in the flame, was measured at 5 pg/mL, similar to the detection limit reported by Riter et al.[20] This is the lowest detection limit ever reported for Pb by LEI using any excitation scheme. The calibration curve was linear over at least 4 orders of magnitude, as is typical of the LEI technique, extending from the detection limit to the point where the transimpedance preamplifier begins to saturate.[25]

Determination of Pb by Laser Ablation and LEI. Figure 6 shows the LEI signal profile for Pb, using the optimal excitation scheme and flame conditions described in the previous sections,

(25) Martin Paquet, P.; Gravel, J.-F.; Nobert, P.; Boudreau, D. *Spectrochim. Acta* **1998**, *53B*, 1907−1917.

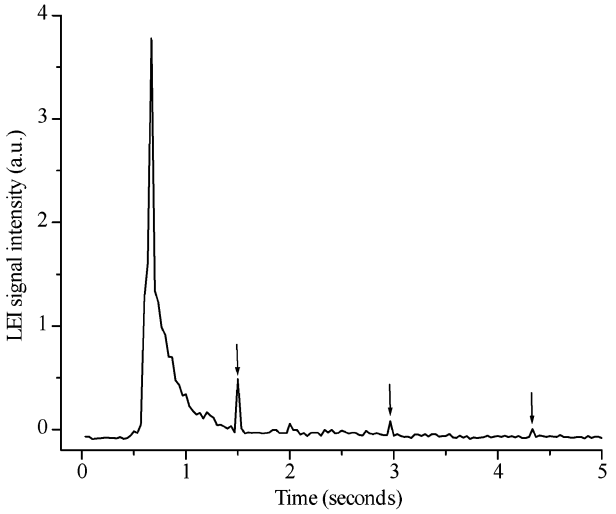

Figure 6. Transient Pb LEI signal from single ablation shot (170 mg/g Pb in Al alloy, 30 Hz detection, 2-step excitation, $Ar-O_2/C_2H_2$ flame).

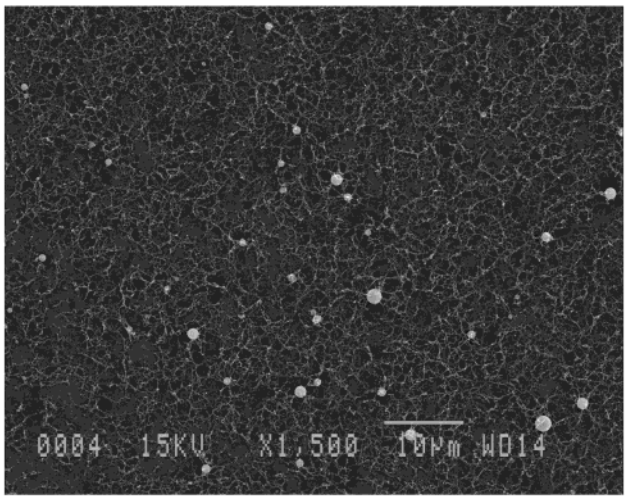

Figure 7. SEM photograph of ablated particles on Nucleopore filter.

for a single ablation pulse onto an aluminum alloy sample containing 170 μg/g of Pb. Given an estimated ejected sample mass of ~20 ng, the total area under the signal trace represents ~3.4 pg of Pb ejected from the sample. The arrows in the Figure indicate short transients in the LEI signals, presumably caused by the passage of larger particles in the flame. Figure 7 shows a scanning electron micrograph of particles collected on a Nucleopore membrane following ablation of an aluminum target using helium as the carrier gas and the setup described in the Experimental Section. From this figure, we see that the ablated particles are of two distinct types, that is, large spherical particles of mostly micrometer size and larger, as well as nanoparticles (<100 nm) assembled as elongated aggregates or filaments. Such filaments have been observed by others[26] and are believed to result from the electrostatic aggregation of nanoparticles created either by hydrodynamic sputtering[26] or by nucleation and condensation of atomic vapor as the expanding plasma meets the ambient gas.[27] The larger particles, on the other hand, are produced either by spallation of the melted layer of target material[26] or by explosive phase change.[28,29] These two types of particles will obviously contribute to a different extent to the analytical signal. On one hand, the smaller aggregated particles will be more efficiently atomized in the LEI flame than the larger particles;[26] on the other hand, the larger particles, while being outnumbered by the smaller ones, may well exceed them in mass. Furthermore, these large particles are more prone to sample losses through gravitational settling during transfer from the ablation cell to the flame detector, possibly leading to a decrease in detection sensitivity.

We have studied the effect of carrier gas composition (helium and argon) on LEI signal intensity and RSD, since it obviously plays an important role in how the particles are generated at the ablation site and how they will be transported to the detection flame. This study was made using a Pb−Sn alloy (55% Pb in weight) and one-step excitation (λ = 283.305 nm), which allowed the use of a very small number of ablation pulses in order to avoid any detrimental effects due to the short depth of field of the ablation optics. For this series of measurements, the LEI signal was measured for each ablation pulse at a detection repetition rate of 30 Hz and integrated over the duration of the ablation transient and averaged over 25 ablation pulses. We observed an increase in LEI signal intensity by a factor of 3 in helium, while the RSD on these measurements is ~3 times smaller (from 31 to 10%, calculated over 25 ablation events). This significant increase in sensitivity has been observed by others using ICP-MS systems,[16,30] who have attributed it to a decrease in redeposition of ablated matter around the crater, rather than to a change in the ejection rate itself, as a result of the greater distance traveled by the ablated material away from the sample surface in the less dense helium atmosphere, therefore resulting in a higher fraction of material able to leave the ablation site. We also have visually observed that less material is redeposited around the craters in helium. Furthermore, the measurements made using the gravimetric procedure described in the Experimental Section show a significant increase of the net ablation yield when using helium as the carrier gas (Figure 8a). On the other hand, the comparison of the average number of pulses required to traverse a thin, flat sample shows a significant increase in helium of the removal rate from the ablation site itself (Figure 8b). These results seem to indicate that not only is the net ablation yield higher in helium, but also that the laser energy reaching the sample surface is higher and that sample material is ejected away from the crater at a greater rate. Such differences in the efficiency of material-laser energy coupling as a function of gas composition have been noted on several occasions, most notably for lasers emitting in the NIR, where they have been attributed to shielding via inverse bremsstrahlung absorption in the plasma created over the surface.[31] In the UV region, however, it is believed that inverse bremsstrahlung, although it cannot be totally discarded, is not as significant and that shielding of the sample surface from an excimer laser beam is due predominantly to Mie extinction

(26) Webb, R.; Dickinson, J.; Exarhos, G. *Appl. Spectrosc.* **1997**, *51*, 707−717.
(27) Callies, G.; Schittenhelm, H.; Berger, P.; Hugel, H. *Appl. Surf. Sci.* **1998**, *127−129*, 134−141.
(28) Song, K. H.; Xu, X. *Appl. Surf. Sci.* **1998**, *127−129*, 111−116.
(29) Yoo, J. H.; Borisov, O. V.; Mao, X.; Russo, R. E. *Anal. Chem.* **2001**, *73*, 2288−2293.
(30) Gunther, D.; Heinrich, C. A. *J. Anal. At. Spectrom.* **1999**, *14*, 1363−1368.
(31) Mao, X. L.; Chan, W. T.; Shannon, M. A.; Russo, R. E. *J. Appl. Phys.* **1993**, *74*, 4915−4922.

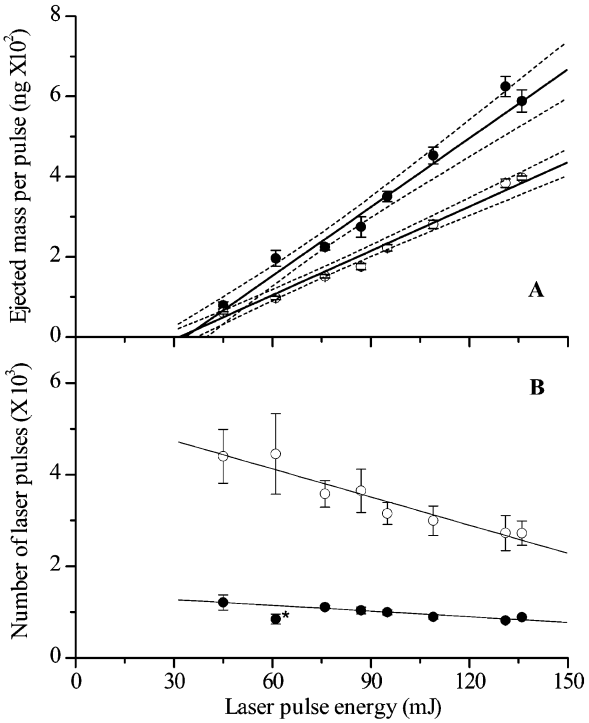

Figure 8. Effect of carrier gas composition (○, argon; ●, helium) on net ablation yield (A) and drilling rate (B) as a function of laser pulse energy (*window of ablation cell was replaced during acquisition of this data point).

(consisting of both absorption and elastic scattering) from particles and clusters formed in the expanding plasma plume.[32] It is unclear which of the absorption or scattering mechanisms predominates in the present work, since this would require knowledge of the particle size distribution in the plasma plume during the laser pulse. Nevertheless, the observation of a higher analytical signal when using helium as ambient atmosphere could result either from a slower cluster growth in the cooler and less dense shock front produced in helium,[27] which could lead to smaller particles, or from a lower particle concentration in the more rapidly expanding plasma plume in the thinner helium atmosphere. Both mechanisms could lead to lessened plasma shielding via Mie extinction and to an increase in ablation yield. Furthermore, the production of smaller particles would also lead to their more efficient atomization in the LEI flame. This second hypothesis is in accordance with the significantly lower RSD values obtained with helium in both LEI signal and in removal rate measurements (Figure 8b), since the unavoidable pulse-to-pulse fluctuations in the number of particles reaching the LEI flame will cause a greater variation of the analytical signal in argon if the upper end of the size distribution (which accounts for a large fraction of the ablated mass) exceeds to a greater extent the size limit tolerated by the flame for efficient particle thermal atomization.

Analytical figures of merit were determined using a continuous sampling procedure, in which 5 different sites of each of the aluminum standards having Pb concentrations between 1 and 170 μg/g were ablated for 30 s at a repetition rate of 30 Hz, and the LEI signal was measured concurrently in the flame also at a

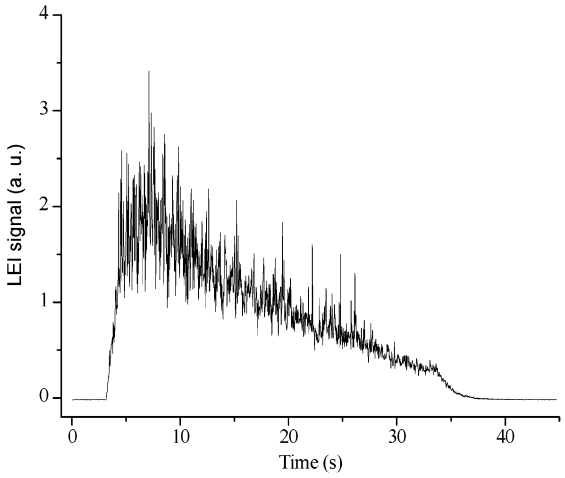

Figure 9. Transient Pb LEI signal from continuous ablation on aluminum sample (170 mg/g Pb in Al alloy, 30 Hz detection, 2-step excitation, Ar−O_2/C_2H_2 flame).

repetition rate of 30 Hz and integrated over the entire signal profile. As has often been reported elsewhere,[33] the recorded signal shows a peak at the beginning of the ablation run (Figure 9); however, because of the short depth of field of the beam imaging optics, the signal does not stabilize to a plateau. This may be a disadvantage of the current ablation setup, as compared to others that use focusing optics of longer focal length, since it may increase the overall RSD on the measured signal. Using this sampling procedure and the 2-step excitation scheme discussed previously ($\lambda_1 = 283.305$ nm, $\lambda_2 = 508.948$ nm), we have calculated a 3σ detection limit of 60 ng/g. This detection limit is ∼4 orders of magnitude poorer than that obtained by introducing Pb directly into the LEI flame using the ultrasonic nebulizer, a decrease in LOD which is very similar to comparative values reported for ICP-MS systems.[34] This decrease is due to a number of factors, but most importantly, to the production by aqueous nebulization of small particles having a narrow size distribution that leads to their more complete atomization and a higher sensitivity, whereas a significant fraction of the sample mass ejected by each ablation pulse is produced in the form of large droplets that exit the atomization source incompletely vaporized. We measured an excellent calibration linearity across the range covered by the aluminum samples that were available to us; however, the linear response range is expected to be larger, since the dynamic range of our experimental setup typically covers over 4 orders of magnitude when measured with aqueous standards. The main limiting factor to the sensitivity attainable with the present setup is the duty factor of the laser system used for detection (4.5×10^{-7}, or 30 Hz × 15 ns), which results in a temporal probing efficiency, given a flame gas linear velocity of ∼390 cm/s and a laser beam diameter in the flame of 3 mm, of 2.3%. The use of a 1 kHz excitation source would therefore decrease the LOD to <3 ng/g.

CONCLUSION

The use of laser-enhanced ionization spectrometry as a detection technique for laser ablation, using a miniature LEI flame

(32) Schittenhelm, H.; Callies, G.; Straub, A.; Berger, P.; Hugel, H. *J. Phys. D* **1998**, *31*, 418−427.

(33) Kleiber, L.; Fink, H.; Niessner, R.; Panne, U. *Anal. Bioanal. Chem.* **2002**, *374*, 109−114.

(34) Pickhardt, C.; Becker, J. S. *Fresenius' J. Anal. Chem.* **2001**, *370*, 534−540.

coupled to an ablation cell and operated with a mixture of argon, oxygen, and acetylene, has been shown to be an extremely sensitive trace elemental analysis technique. Using the two-step excitation scheme ($6p^2\ ^3P_0 \rightarrow 6p7s\ ^3P_1^\circ \rightarrow 6p9p\ ^3P_2$), a detection limit of 5 pg/mL was obtained for direct nebulization of Pb aqueous solutions into the flame, and a laser ablation detection limit of 60 ng/g was obtained for the determination of Pb in aluminum samples. The use of helium as ambient atmosphere in the ablation cell and as carrier gas for the ablated material provided greatly enhanced detection sensitivity and ablation pulse-to-pulse repeatability, as compared to the use of argon. The main limitation to the current experimental setup is the modest probing efficiency, which could be increased by the use of a higher repetition rate solid-state pump laser. Another factor that may well be hindering the sensitivity is the limited atomization capability of the miniature LEI flame toward larger particles, and this aspect of the technique deserves closer examination. The present work is the first one to date to report analytical figures of merit for the coupling of laser ablation and LEI; however, it is worthwhile to compare the results obtained herein with those published by Riter et al. who combined graphite furnace vaporization with LEI detection to determine the concentration of Pb in diluted blood microsamples.[10] Using this technique, they obtained a 3σ detection limit of 42 fg of Pb in a 10-μL sample volume. In a similar fashion, recent work in our group with the GF-LEI technique has demonstrated the detection of Pb as an impurity in pyrolytic graphite at a level of 70 fg.[35] Whereas the temporal probing efficiency in these experiments was also limited by the modest duty factors of low repetition rate pump lasers, the better repeatability of the graphite furnace from vaporization cycle to vaporization cycle (as compared with laser ablation) and, most of all, the very small size of the particles presented to the miniature LEI flame resulted in phenomenal detection capabilities. We believe that further development of the LA-LEI technique will lead to such detection capabilities and to unique applications such as single-shot trace analysis of heterogeneous solid samples surfaces with micrometer-scale lateral and depth resolution.

ACKNOWLEDGMENT

We are grateful to the Natural Sciences and Engineering Research Council of Canada (NSERC) and the "Fonds Québécois de Recherche sur la Nature et les Technologies" (FQRNT) for financial support of this research. J.-F.G. is indebted to the Fondation de l'Université Laval for financial support. The authors also express their gratitude to Dr. Marc Choquette, of the Laboratoire de Microanalyse de l'Université Laval, for his assistance with the SEM measurements used in this work.

Received for review October 9, 2002. Accepted January 14, 2003.

AC026223K

(35) Nobert, P.; Herreyre, K.; Boudreau, D. *25th FACSS Meeting*, Detroit, MI, October 2001.